Beyond Steady-State: Dynamic Modelling of Cavern–Grid Interaction for Resilient Hydrogen Infrastructure Design

Lars Höpken[a], Wiebke Germer[a], Hendrik Langnickel[a], Alexander Dyck[a], Carsten Agert[a]

[a] *German Aerospace Center (DLR), Institute of Networked Energy Systems, Carl-von-Ossietzky-Str. 15, 26129, Oldenburg, Germany*

Abstract

Fluctuating hydrogen supply and demand challenge future infrastructure, making large-scale hydrogen storage indispensable. Many scenarios forecast German capacities of up to 80 TWh. However, these often use steady-state simulations, which estimate overall storage requirements but cannot capture technical interactions between grids and storages. This study presents a dynamic model to re-examine future scenarios and systematically assess the storage-grid interaction within the German hydrogen core network. The results reveal that grid constraints limit the storage's balancing capability and lead to significant load shedding and supply curtailment. More precisely, both the deliverable power to a grid section and the time lag between storage discharge and availability of additional flow strongly depend on the spatial distance and the diameter of the connecting pipeline. In combination with limited line pack availability, certain scenario conditions become infeasible. Dynamic simulation and combined consideration of grid and storages is therefore essential for planning resilient hydrogen infrastructure.

Keywords: hydrogen grid, dynamic gas network simulation, cavern storage, storage-grid interaction, line pack

1. Introduction

With the approval of the hydrogen core network in Germany [1], the first step towards a large-scale hydrogen infrastructure and economy has been made. The grid is designed to connect all major regions of supply and demand within Germany and consists of more than 9,000 km of pipelines [2]. It integrates into the larger European Hydrogen Backbone (EHB) [3], serving an important role in pan-European, renewable energy provision.

A major challenge for this future hydrogen infrastructure is the volatile production via electrolysis using renewable electricity. In this context, establishing a reliable and secure hydrogen system requires large-scale storages and several studies calculate a future storage capacity of up to 80 TWh for Germany alone [4, 5, 6]. This storage demand will primarily be provided by salt caverns due to the large geologic potential [7]. On account of the altered boundary conditions, new requirements for the systems involved compared to state-of-the-art natural gas operation will arise [8]. Here, projects like FrHyGe [9], Hydrogen Cavern for Mobility (HyCavMobil) [10] and H2 CAvern Storage Transition (H2CAST) [11] aim to quantify these requirements and demonstrate the storage of hydrogen in salt caverns. The latter is realised at the cavern site in Etzel in north-west Germany, an important hub for the future European hydrogen infrastructure.

Höpken et. al. [8] previously investigated the impacts of different compositions of renewable energy sources (RES) on the available electricity for hydrogen production and the resulting storage demand. It was suggested to include the transmission network in further research to obtain more accurate storage requirements. Similarly, the association of German gas and hydrogen storage system operators (INES) criticised the design of the core grid to not sufficiently consider the role of storages and their importance for balancing purposes [12], highlighting the need to assess storages and grid together. Most scenario studies, like the ones listed above, rely on steady-state simulations to optimize these coupled systems. However, steady-state models are unable to capture the technical interaction between the grid and storages, making them unsuitable for detailed analyses. For this purpose, a coupled dynamic model of the gas network and the cavern model introduced in [8]

Email address: hendrik.langnickel@dlr.de (Hendrik Langnickel)

is developed and utilized to explore this interaction. Emphasis is put on the employment of a grid model which is dynamic, since this enables the consideration of the buffering capability of the pipeline volume, known as line pack, as well as transient behaviour due to fast changes in boundary conditions. While these two grid characteristics do not significantly affect storage capacity, they substantially influence storage operation and balancing capabilities.

The aim of this study is to quantify these influences based on the example of cavern storage in Etzel that is connected to the German hydrogen core network and thus gain a deeper understanding of relevant parameters for a resilient system design under dynamic conditions. First, the model ecosystem is introduced. In the following chapter, a scenario use case is modelled and analysed. Finally, a more general approach is applied in order to examine the storage-grid interaction in a systematic way.

2. Methodology

This section introduces the developed gas network model and describes the coupling mechanism to the existing cavern model. Next, the assessed scenario is defined and the used dispatch logic for solving infeasibilities is explained.

2.1. Dynamic gas network model

The key difference between steady-state and dynamic network models is the ability to model imbalances and their impact on the system. Steady-state simulation always enforces equilibrium and therefore does not consider the duration of a time step or the previous grid state. In contrast, dynamic modelling takes these factors into account and enables, for example, the assessment of state changes due to imbalanced loads and supplies, as well as the propagation of pressure changes over time.

Several commercial dynamic gas network simulation tools already exist on the market. Some of the most popular ones are SIMONE [13], PSIganesi [14] and SAInt [15]. However, due to their closed architecture they cannot easily be expanded and coupled with other models. For this reason, open-source software is to be preferred. Currently available open-source gas network models include pandapipes [16] and GasNetSim [17]. Both of these do not support dynamic simulation at the moment and thus are unsuitable for the analyses in this study. The literature describes several dynamic models, each with a different focus. Chen et. al. [18] implement simultaneous hydraulic simulation and component tracking with a decoupled model. Lu et. al. [19] also consider component tracking but make use of an electrical analogy model. This analogy is also applied by Huang et al. [20]. Zhou et. al. [21] use machine learning algorithms in order to reduce uncertainty due to the high non-linearities in gas pipeline systems. Burlacu et al. [22] and Hari et al. [23] introduce solutions to the non-linear control problem of optimal gas network operation. Pambour et al. [24] present a transient gas network model that includes ancillary infrastructure. All of these publications do not share the source code of the dynamic models they publish. For this reason, a new dynamic gas network simulation tool called DLR-DUST is developed. Contrary to some of the listed models, DLR-DUST applies hydraulic principles and physical fluid properties instead of heuristic or equivalence methods. The new development further brings the added benefit of incorporating the coupling mechanism with the cavern model directly from the beginning, allowing bi-directional exchange and constraint handling.

2.1.1. Model description

DLR-DUST is a dynamic simulation software package written in Python for gas networks and associated infrastructure. It enables the realistic modelling of freely definable gas networks and provides, amongst other things, pressures, volume flows, flow velocities and friction losses during operation. A key functionality is the integration of transient behaviour like the gas's inertia and the storage capacity of the pipelines (line pack). In its simplest configuration, the model consists of only nodes and pipes. The pipes transport the gas between the nodes and make up the volume of the grid. The nodes connect to one or more pipelines and can also extract or withdraw gas from the network and thus serve as sinks or sources.

The governing equations and general model structure are based on Pambour [24, 25]. While some essential definitions are presented in the following, the reader is referred to the original sources for in-depth information.

At its core, the network model consists of the following three categories of equations. Equation (1) shows the continuity equation for each node of the network i after an implicit time integration for a time step $\Delta t = t^{n+1} - t^n$ (see Eq. (25) and following in [24]). It connects the change in pressure $p^{n+1} - p^n$ in the nodal volume V with the load L and the incoming and outgoing flows Q of the k connected pipes. The nodal volume aggregates the halves of the volumes of all connected pipe segments. ρ_n is the density at standard conditions of the fluid and c is the speed of sound at the current fluid conditions. The factor a indicates whether node i is the inlet or outlet of pipe j by being either plus or minus 1. Separating the terms by current and future time step yields the shown structure.

$$\frac{V_i}{\rho_n c_i^2 \Delta t} p_i^{n+1} - \sum_{j=1}^{k} a_{i,j} Q_j^{n+1} + L_i^{n+1} = \frac{V_i}{\rho_n c_i^2 \Delta t} p_i^n \tag{1}$$

A direct consequence of modelling the pressure inside the nodal volume is the ability of considering line pack. In a steady-state setting, the time step Δt would approach infinity to ensure equilibrium and thus enforce a balance between the load and the sum of all pipe flows.

The second type of equations is the linearized pipe equation (2), which is formulated for every pipe in the network (Eq. (16) and following in [24]). It is obtained from a set of partial differential equations, namely a continuity, momentum, energy and a state equation. By assuming isothermal flow and neglecting convection, the set can be simplified and linearized around a given point. Since the linearization is only accurate close to the reference point, it is repeatedly solved in an iterative process with k steps. The indices *in* and *out* represent inlet and outlet of the pipe segment, while R_f and R_i are the resistance coefficients from friction and inertia, respectively. The variable s is a correction factor for altitude differences between the pipe's ends.

$$p_{in,j}^{k+1,n+1} - p_{out,j}^{k+1,n+1} e^{s/2} - \frac{2R_f |Q_j^{k,n+1}| + R_i}{p_{in,j}^{k,n+1} + p_{out,j}^{k,n+1} e^{s/2}} Q_j^{k+1,n+1} = - \frac{R_f |Q_j|^{k,n+1} Q_j^{k,n+1} + R_i Q_j^n}{p_{in,j}^{k,n+1} + p_{out,j}^{k,n+1} e^{s/2}} \tag{2}$$

Looking at the inertia term on the right side of the equal sign, the dependence on the previous flow Q^n is visible. This is most relevant for large changes in flow from one time step to the next, as the fluid has to overcome a lot of inertia. When no changes occur, the term cancels with the left side.

The third type of equations defines the boundary conditions of the network by setting the values in equations (3) and (4) (see Eq. (30) and (31) in [24]). Equation (3) acts as a control input for non-pipe elements such as compressors. Depending on the control mode, the variables c_1, c_2, c_3 and d are used to define the element's operating condition. Pambour summarises possible inputs in [25] in table 2.5.

$$c_{1,j} \cdot p_{in,j}^{n+1} + c_{2,j} \cdot p_{out,j}^{n+1} + c_{3,j} \cdot Q_j^{n+1} = d_j \tag{3}$$

Extending Pambour's methodology, DLR-DUST also allows the use of this equation for pipe control. This is beneficial for limiting e.g. the flow velocity inside certain pipelines. Equation (4) represents the node controls. The scalars k_p and k_L equal either 0 or 1, depending on whether a pressure or load control is described. The control value is determined by the variable b.

$$k_{p,i} \cdot p_i^{n+1} + k_{L,i} \cdot L_i^{n+1} = b_i \tag{4}$$

For a solvable system the number of linearly independent control equations has to match the number of nodes plus the number of non-pipe elements in the network. Contrary to the implementation by Pambour [25], this does not enforce each node being either pressure or load controlled, but also allows setups where a node might be both pressure and load controlled if another node or element is completely undefined. In the context of storage coupling this is advantageous since the storage site might define both parameters.

Formulating all equations for a given network results in a set that can be written as a linear matrix equation (5) in the form $\mathbf{A} \cdot \mathrm{x} = \mathrm{b}$ (similar to Eq. (32) in [24]). The system can be solved for the x-vector, which contains all pressures, flows and loads of the next time step. The matrix $\mathbf{A}$ is of size $(2n_n + n_N + n_P) \times (2n_n + n_N + n_P)$ with n_n being the number of nodes, n_N the number of non-pipe elements and n_P the number of pipes. It consists of several sub-matrices corresponding to equations (1), (2), (3) and (4). $\mathbf{\Phi}$ is a diagonal matrix of the pressure coefficients, $\mathbf{A_P}$ is the node-pipe incidence matrix, $\mathbf{A_N}$ the node-non-pipe incidence matrix and $\mathbf{I}$ the identity matrix. In the second row, $\mathbf{A_{DP}}$ is the pipe-node incidence matrix including the pressure drop term from height differences and $\mathbf{R}$ is a diagonal matrix of the slopes of the linearized pipe equations. Finally, $\mathbf{D_p}$, $\mathbf{D_Q}$, $\mathbf{C_p}$, $\mathbf{C_Q}$, $\mathbf{K_p}$ and $\mathbf{K_L}$ are the pressure, flow and load control matrices of pipes ($\mathbf{D}$), non-pipe elements ($\mathbf{C}$) and nodes ($\mathbf{K}$). After the equal sign, the b-vector consists of the vectorised right sides of the previous equations.

$$\begin{pmatrix} \mathbf{\Phi} & -\mathbf{A_P} & -\mathbf{A_N} & \mathbf{I} \\ \mathbf{A_{DP}} & -\mathbf{R} & \mathbf{0} & \mathbf{0} \\ \mathbf{D_p} & \mathbf{D_Q} & \mathbf{0} & \mathbf{0} \\ \mathbf{C_p} & \mathbf{0} & \mathbf{C_Q} & \mathbf{0} \\ \mathbf{K_p} & \mathbf{0} & \mathbf{0} & \mathbf{K_L} \end{pmatrix} \begin{pmatrix} p^{n+1} \\ Q_P^{n+1} \\ Q_N^{n+1} \\ L^{n+1} \end{pmatrix} = \begin{pmatrix} \mathbf{\Phi} p^n \\ B \\ F \\ E \\ S \end{pmatrix} \tag{5}$$

In order to increase the accuracy of the simulation, long pipes can be discretised into smaller segments. This reduces the error from linearisation, assigning pipe volumes to the closest node and averaging fluid properties along pipes. However, the increased accuracy is computationally expensive. Doubling the number of pipes also adds another n_P nodes to the network where the segmented pipes are connected. Thus, the matrix dimensions become $(2(n_n + n_P) + n_N + 2n_P)^2$. Assuming $n_n = n_P$ and $n_N = 0$ yields a two-fold increase in both dimensions. Since solving a matrix equation has a complexity of at least $O(n^2)$ [26], the computation time increases by a factor of at least four.

For each time step of the simulation DLR-DUST builds the matrix from equation (5) and computes the result. Because of the linearized pipe equation, this solution requires reiteration until the results converge. In order to determine convergence, the residual vector Res is defined as the euclidean norm of the change in the results vector x after the last iteration step $k + 1$ (Eq. 6).

$$Res = \sqrt{\sum_{i=1}^{2n_n+n_N+n_P} (x_i^{k+1} - x_i^k)^2} \qquad (6)$$

Once this residual falls below a given tolerance, the results are saved and the next time step is simulated.

The presented hydraulic equations require a broad spectrum of fluid property data. Precise values are therefore vital for accurate simulation results. Since most fluid properties depend on the pressure and temperature conditions, these values have to be obtained during simulation. Here, DLR-DUST makes use of the Python wrapper for CoolProp [27]. It utilizes the Helmholtz Equation of State (HEOS) to obtain densities, compressibility factors, specific heat capacities, enthalpies, viscosities, thermal conductivities and expansion coefficients for every element in the network during each iteration. The versatility of CoolProp also allows DLR-DUST to work with many different gases and gas mixtures.

2.1.2. Validation

DLR-DUST is benchmarked against the commercial software SAInt [15], which itself has been validated against SIMONE [13] and other transient models [24]. The validation uses the 25-node sample network from [25] and the input data provided in its appendix. This network features 18 demand nodes, a single supply node (node 1) and three compressors located at nodes 5, 13 and 16 (Figure 1). Each demand node uses a scaled 24-hour load profile which is also shown in [25]. Node 1 is set to a pressure control of 50 bar and injects into the grid accordingly. The three compressors operate dynamically to always provide an outlet pressure of 55 bar. In this case, the fluid is methane.

As the dynamic simulation requires an initial solution, the first step is calculated using the steady-state model. The resulting pressure distribution in the network is shown in Figure 1. Further, the flow direction in the pipes can be derived from the pressure differences between the end points of each pipe.

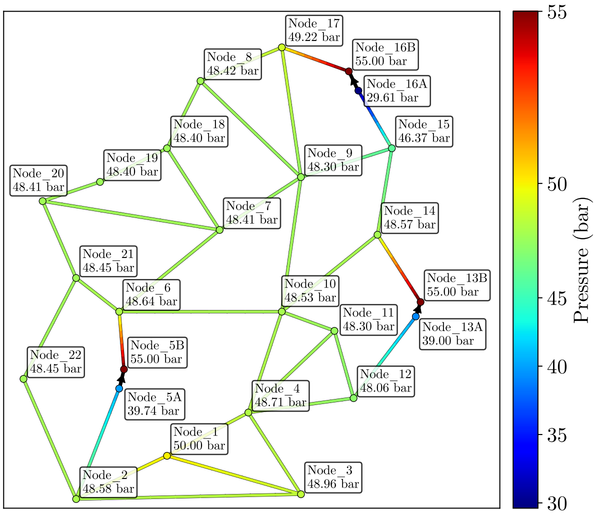

Figure 1: Initial steady-state pressure solution of the 25-node sample network obtained from DLR-DUST

Starting from this initial state, the simulation runs the 24-hour scenario in a 15-minute resolution. After discretisation, the system consists of 94 nodes and 104 pipes. Solving takes around 0.3 s on laptop hardware. The results plotted in Figure 2 show overall good agreement between the dynamic simulation of DLR-DUST (black) and the output of SAInt (red). While the injection at node 1 (subplot a) and the flow through the pipe connecting nodes 4 and 11 (subplot c) are almost indistinguishable, the pressure at node 9 exhibits a minor deviation of up to 0.2 bar. Since the offset is rather constant, it can be attributed to slight differences in fluid property calculation between the two models and is deemed negligible.

In addition to the dynamic comparison, the blue line shows the results from steady-state simulation. As to be expected, the curves start from the same point, since the dynamic model uses a steady-state solution as its initial conditions. For the remainder of the simulated time

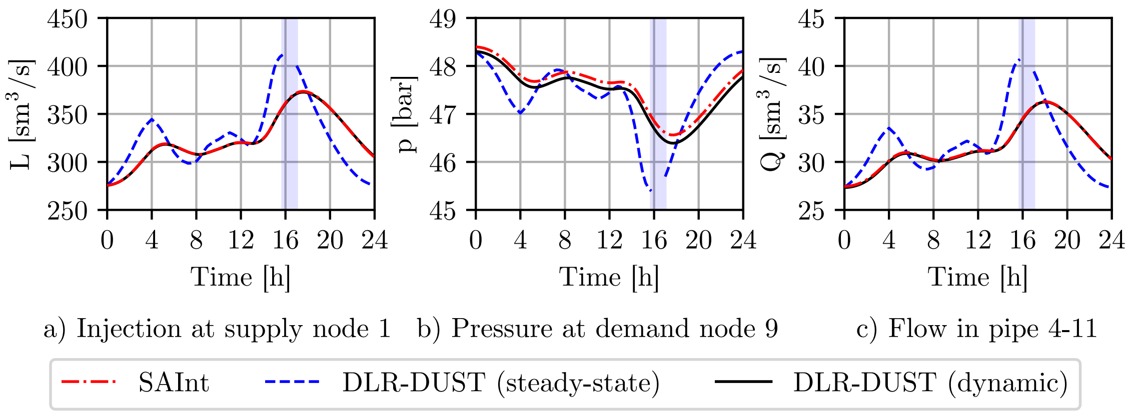

Figure 2: Comparison of simulation results at selected elements of the sample network between SAInt and DLR-DUST. The blue bars indicate infeasibilities in the steady-state solution.

frame, the steady-state results exhibit major deviations from the dynamic results and appear to be more volatile due to higher-amplitude changes. Furthermore, the peaks and valleys of the dynamic curves are delayed by about one hour. This behaviour highlights the effect of the buffering capability of the network's line pack volume and demonstrates the importance of dynamic models for realistic simulation of flow and pressure conditions. For some hours of the test scenario, the steady-state solution even becomes infeasible due to insufficient pressure in parts of the network. These hours are marked by the blue shaded areas in Figure 2.

2.2. Coupling of network and cavern model

In order to enable detailed analyses of the storage-grid interaction, DLR-DUST is coupled with the numerical cavern model from [8]. The system boundaries of the two models are the cavern head on the storage side and the grid connection point on the network side. At each of these boundaries exists an interface where a gas volume flow can enter or exit the model. However, the two flow interfaces cannot be connected directly. Instead, they require a surface facility that handles pressure, temperature and potentially gas quality alignment. To achieve this, surface facilities typically consist of compressors, pressure regulators, heat exchangers and gas treatment equipment.

2.2.1. Surface facility model

For the purposes of this study, a simplified surface facility model is introduced. The schematic in Figure 3 shows the structure of the model and flow directions for different operating modes. During simulation, the three core components, compressor, heat exchanger and expansion valve, perform the task of aligning pressure and temperature conditions between the cavern head (4) and the grid connection point (1).

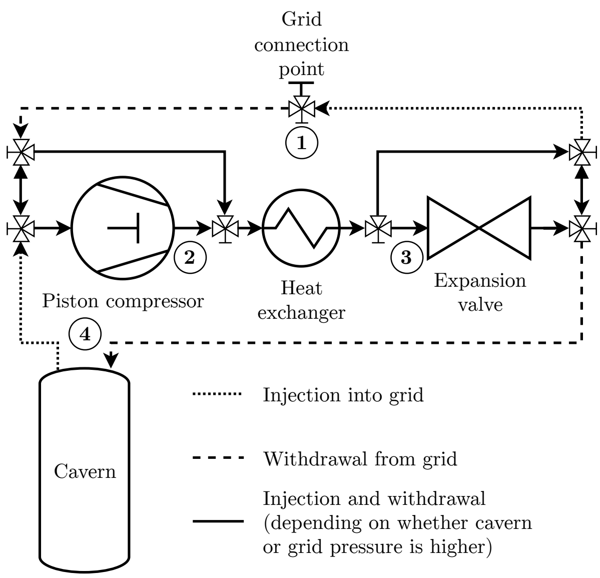

Figure 3: Schematic of the simplified surface facility model connecting the cavern model to DLR-DUST

The compressor is modelled as an idealised isentropic change of state. Using CoolProp [27], the enthalpy $h_{in}(p_{in}, T_{in})$ and entropy $s_{in}(p_{in}, T_{in})$ are obtained from the know inlet gas state. With the isentropic condition $s_{in} = s_{out}$, the outlet temperature $T_{out}(p_{out}, s_{out})$ and enthalpy $h_{out}(p_{out}, s_{out})$ can be determined. Finally, the ideal, isentropic compressor power is calculated according to equation (7) with $\dot{m}$ being the mass flow [28].

$$P_{comp} = \dot{m}(h_{comp,out} - h_{comp,in}) \tag{7}$$

For the heat exchanger, the model assumes an ideal process without pressure loss ($p_{out} = p_{in}$). After calculating the enthalpies $h_{in}(p_{in}, T_{in})$ and $h_{out}(p_{out}, T_{out})$, equation (8) is used to obtain the heat flux [28].

$$\dot{Q}_{hex} = \dot{m}(h_{hex,out} - h_{hex,in}) \tag{8}$$

Pressure reduction between cavern and grid is achieved via an isenthalpic expansion valve. Contrary to the compressor, it is not the outlet conditions that are unknown, but rather the necessary input temperature to achieve either grid or cavern compatible states. From the know outlet conditions, the enthalpy $h_{out}(p_{out}, T_{out})$ can be determined. Since $h_{in} = h_{out}$ and p_{in} is also known, $T_{in}(h_{in}, p_{in})$ is obtainable from CoolProp.

2.2.2. Coupling logic

As the arrows in Figure 3 suggest, the utilization of the facility's sub-components is dependent on the direction of flow and the pressure conditions. Typically, the pressure in the cavern exceeds the grid pressure. If that is the case and stored hydrogen from the cavern is injected into the grid, the gas flows from (4) to (3) to (1). Here, the cavern model defines the gas state at the cavern head (4) and the network model sets the required pressure at the grid connection point (1). Since the grid temperature is constant (typically 12 °C), the only unknown is the state before expansion (3) and the required heat flux in the heat exchanger. This amount also depends on the temperature change in the valve which is a function of the Joule-Thomson coefficient of the utilized gas.

In the reverse case, when gas is withdrawn from the grid and stored in the cavern, it will follow the path from (1) to (2) to (4). Again, the states at (1) and (4) are defined. The only exception is the temperature at the cavern head. In this case, the target temperature for cavern injection is set to 50 °C. From this, the surface facility model calculates the gas state at position (2) and the necessary compression and cooling powers using equations (7) and (8).

For the rare case of a higher grid pressure compared to the cavern pressure, the gas flow will follow (4)-(2)-(1) and (1)-(3)-(4) for grid injection and withdrawal, respectively.

Most of the time, a storage site will consist of more than a single cavern. While it is possible to split the flow between caverns in different ways, the default assumption is simultaneous operation of all caverns. In that case, only one of them will be simulated in order to reduce redundancy and improve performance. The results then represent the conditions for all equally operated caverns.

2.3. Scenario definition

The focus of this study lies on the dynamic assessment of the future German hydrogen infrastructure. Its backbone is the core network, which is set to be finished by 2037 at the latest [2]. The published version of the network contains detailed information about each pipeline, including length and diameter. This data is collected and combined with altitude information from a digital terrain model [29] and bathymetry data [30] in order to respect height differences between sections of the grid. The roughness of the pipes is assumed to universally be 0.1 mm. Table 1 gives an overview of the resulting simulation inputs. The final network consists of 282 nodes and 330 pipes with a total length of around 9,000 km. As most pipelines lie underground, the grid temperature is set to 12 °C. The used fluid is 100 % hydrogen.

Contrary to the core network, no clear pathway for the construction of underground hydrogen storage exists yet and amount as well as locations are undetermined. Since Etzel in north-west Germany is an established site for large scale natural gas storage and the repurposing of existing salt caverns for hydrogen use is already being tested in the project H2CAST [11], this site is chosen as storage location for the scenario. The exemplary cavern used in the coupled model is cavern A from [8] and uses the same input data.

Besides the infrastructure, additional scenario inputs are required. As listed on the right side of Table 1, the year of targeted climate neutrality, 2045 [31], is chosen for the analysis. The report [4] of the long-term scenarios 3 [32] provides the overall hydrogen supply and demand as well as the distribution between import and electrolysis as well as the demand sectors. The O45-power scenario, which assumes high electrification, states an import share of 57 % and exclusive demand in the sectors industry and energy (power plants). The total demand adds up to 305 TWh (see Table 1). For the simulation, these values have to be regionally distributed and associated with hourly profiles. Within the project TransHyDE [33], the demands of different sectors, as well as production from electrolysis until 2050 have been modelled with a NUTS-3 spatial and

Table 1: Overview of simulation inputs

Infrastructure inputs		**Scenario inputs**	
Number of nodes	282	Year	2045
Number of pipes	330	Number of time steps	8760
Total pipeline length	8998.5 km	Length of one time step	1 h
Total pipeline volume	5.679 Mil. m^3	H_2 supply: Electrolysis	131 TWh
Roughness	0.1 mm	H_2 supply: Import	174 TWh
Grid temperature	12 °C	H_2 demand: Industry sector	201 TWh
Cavern injection temperature	50 °C	H_2 demand: Energy sector	104 TWh

hourly temporal resolution. The data is publicly available on the FfE Open Data Portal [34]. This study uses the 2045 profiles of the industry sector [35] and for electrolysis [36] and scales them to the long-term scenario totals. Import and energy sector profiles are taken from the hydrogen dispatch dashboard of the long-term scenarios [37]. Figure 4 shows the resulting annual profiles.

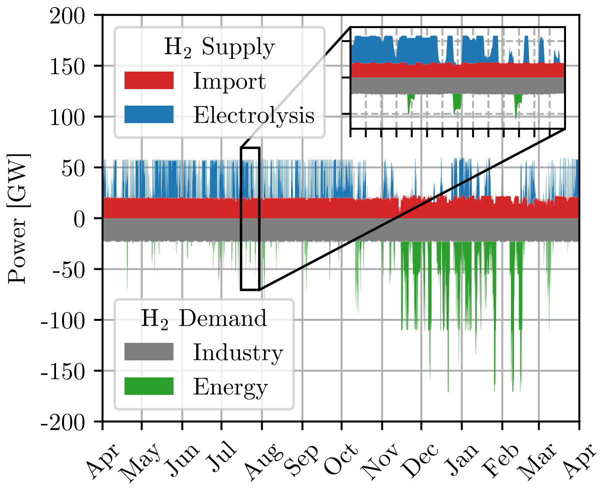

Figure 4: Profiles of hydrogen supply and demand for Germany in 2045 [35, 36, 37]

Applying the regional distribution from TransHyDE yields the maps in the top row of Figure 5 for hydrogen supply and demand. Darker colours represent regions of high supply or demand. While hydrogen generation is stronger in the North due to large wind capacities, demand is concentrated around industry clusters in the east and west, as well as bigger cities. Since not all districts are intersected by a pipeline of the core network, the data has to be modified. Assuming that the regions in question are served by distribution grids that connect to the transmission grid, the original map is ”condensed” onto the core network with the following steps:

1. Find the closest pipeline to the unconnected district
2. Of the start and end node, find the closer one
3. Determine the district the node lies in
4. Add the data of the unconnected district to this district

After condensation, the distributions change as shown in the bottom row of Figure 5.

In many cases there is more than one node inside a district. DLR-DUST however requires supplies and demands per node. To split the total load across nodes in a realistic way, each node gets assigned its maximum connected pipeline capacity. This value depends on the diameter of the largest pipeline the node is connected to. The load is then distributed proportionally to this value, preventing overloading of small pipelines. Lastly, the conversion from power (GW) to hydrogen standard volume flow (sm^3/s) is done with a lower heating value of 3 kWh/sm^3.

2.4. Dispatch

One of the most challenging aspects of dynamic gas network simulation is management of the dispatch. Since line pack adds a degree of freedom to the system compared to steady-state modelling, the control becomes more complex and non-linearities complicate optimization ([22, 23]). In this work, a simple, curtailment-based approach is pursued for demonstration purposes but might be replaced by more sophisticated control algorithms in the future.

The key problem, the control algorithm has to solve, is the management of imbalances in the grid and simultaneous adherence to valid operating conditions. The operative boundaries of the grid are defined in a list of constraints. In this example, it consists of a minimum and a maximum pressure of 50 and 70 bar, respectively, at each node of the network. By default, each node is controlled by the supply or demand profile it got assigned. The only exception is Etzel, where the storage

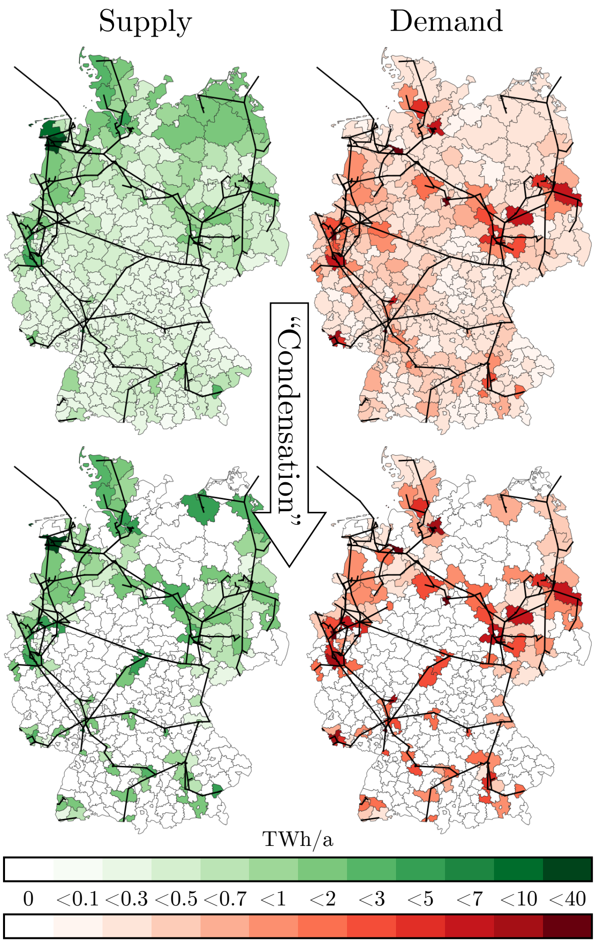

Figure 5: Distribution of hydrogen supply and demand with NUTS-3 resolution before and after condensation onto the German core network (black) [35, 36]

site is connected. Its control is set to a nominal grid pressure of 60 bar. During each time step, the network is first solved with its default controls. Following that, the result is analysed for constraint violations (i.e. pressures outside the allowed range). In case no violations are found, the next time step is initiated. If there are violations, the dispatch tries to resolve them through curtailment and load shedding. For this, the algorithm collects all nodes where a violation occurred and divides them into minimum and maximum pressure violations. For each minimum pressure violation it finds the closest load (oftentimes the exact node of the violation) and for each maximum pressure violation the closest supply. The identified loads and supplies are then reduced in a stepwise process until no violations are left. In case a load or supply is curtailed to zero, this control is marked undispatchable in order to prevent sinks from becoming sources and vice versa. The algorithm then uses the next closest control to solve the violation. In this manner, all constraints can be adhered to, while keeping curtailment or load shedding as low as possible.

Since each adjustment of a control value requires re-solving of the network, the dispatch is computationally intensive and overall simulation time strongly depends on the necessary re-dispatch of the original set of controls.

3. Dynamic simulation of long-term scenario

This section presents the results from dynamic simulation of the test scenario defined in section 2.3 with DLR-DUST. The dispatch (section 2.4) ensures maximum utilization of the core network's capacities while adhering to the pressure constraints of 50 to 70 bar. Simultaneously, the single storage site in Etzel is used to maintain a local pressure of 60 bar. It comprises several caverns of which only one is simulated as a representation of cavern operation at this location.

From the balance-sheet point of view of the test scenario, hydrogen supply and demand are perfectly balanced. However, running the simulation reveals substantial overloading of the network and subsequent load shedding and curtailment. Figure 6 shows the spatial distribution of shedded loads and their amplitude. While load shedding is prevalent across the entire grid, industry centres with high demand are most affected (note the logarithmic scale of the markers). In total, the unsatisfied demand amounts to around 64 TWh, which is 21 % of the combined annual total.

Load shedding occurs due to under-pressure in the grid. In order to investigate the causing segments, the amount of time each pipeline spends within 0.1 bar of the minimum pressure is displayed in blue. Many of these critical pipeline segments are located in southern Germany, far away from Etzel. This hints at the inability of the storage's pressure regulation to reach these locations and load shedding becoming inevitable. Additionally, two other regions of frequent under-pressure can be observed. One in the central West and one just south-east of Etzel. Both of these are locations with very high demand (compare Fig. 5) which seems to overload the local pipeline infrastructure. Load shedding outside of these areas can be explained by short term pressure violations, as well as collateral effects when the load shedding in the critical regions is not sufficient.

Analysing the time series in Figure 6 reveals a direct correlation of the amount of load shedding and the

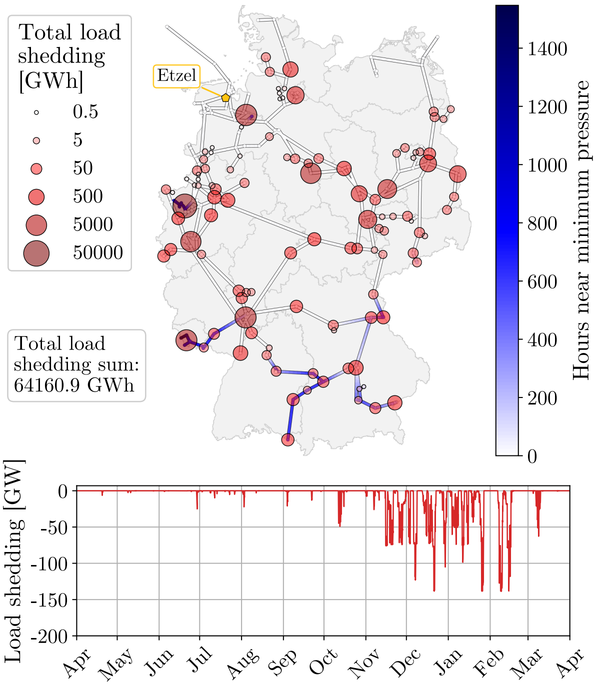

Figure 6: Spatially and temporally resolved load shedding (red) in the test scenario with the underlying critical pipeline segments (blue). Note that some points have been aggregated for better visibility.

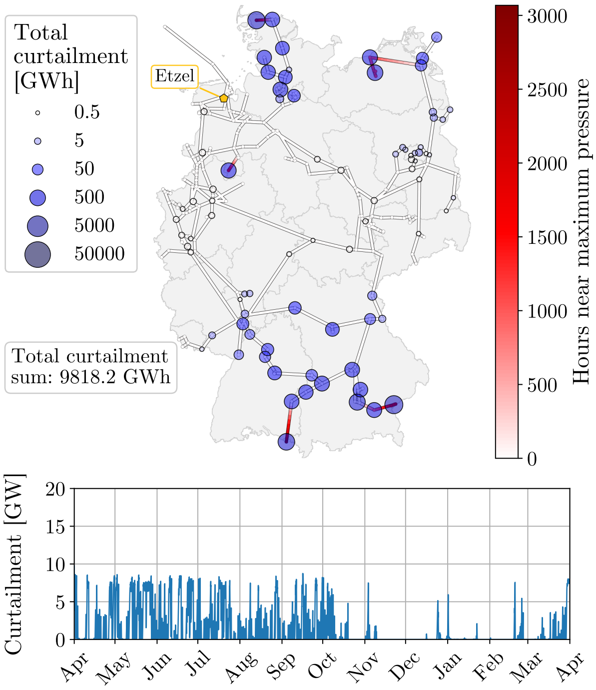

Figure 7: Spatially and temporally resolved curtailment (blue) in the test scenario with the underlying critical pipeline segments (red). Note that some points have been aggregated for better visibility

demand of the energy sector (Fig. 4). The volatility and high amplitudes of demand spikes of hydrogen power plants oftentimes cannot be served by the grid in the given configuration and therefore have to be curtailed.

On the opposite side, hydrogen supply is a lot more uniform. Consequently, this leads to lower curtailment on the supply side, which is shown in Figure 7. The time series remains below 10 GW at all times and the curtailment adds up to around 10 TWh, which is just 3 % of the total amount.

The spatial distribution also shows a different pattern with major curtailment occurring in the very North and South of the country. While the North has high generation capacities and therefore overloads the network at times, the South again suffers from the long distance to Etzel. The highlighted pipeline segments with frequent pressures above 69.9 bar confirm this relation with the outermost segments being most affected. In the South, the collateral supply curtailment around these regions is also clearly visible.

The coupled cavern model receives the injection and withdrawal profile at Etzel and scales it to the size of a single cavern (Cavern A in [8]). It therefore represents the necessary average cavern operation at this location.

As shown by the pressure profile in Figure 8, the storage is not balanced over the simulated year. This is a result of the large mismatch between load shedding and supply curtailment, with the latter being affected less and thus leading to a mostly filled storage at the end of the cavern year. The rock temperature reflects this as well, being around two degrees higher at the end due to less withdrawal cooling the cavern content. A consequence of this is that in the following years less storage capacity is available and supply curtailment will catch up to load shedding in total amounts.

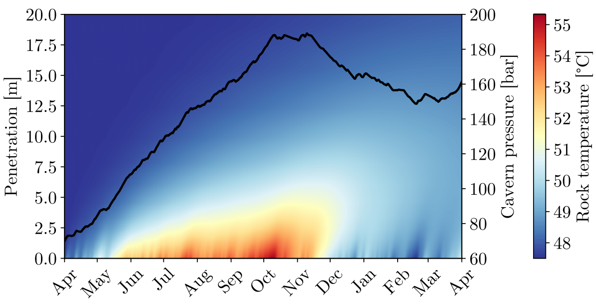

Figure 8: Pressure profile (black) in the exemplary cavern during the test scenario and the resulting temperature distribution in the salt rock

For comparative purposes, the test scenario is also simulated in two other configurations. Firstly, DLR-DUST is set to steady-state mode with otherwise identical inputs. Secondly, it is switched back to dynamic and the storage is removed entirely in order to obtain a baseline of curtailment and load shedding. The results of theses simulations are shown in Table 2. Analysing the differences between the default configuration and the steady-state case reveals the buffering capability of line pack which prevents around 7 TWh of load shedding and around 11 TWh of curtailment. This once again emphasises the relevance of dynamic simulation for these analyses. Removing the storage from the system results in load shedding of more than 88 TWh and curtailment of more than 84 TWh. The significant difference to the previously shown results quantifies the balancing capability of a well-connected storage site like Etzel. While load shedding is reduced by around 27 %, supply curtailment decreases by more than 88 %. As stated before, for subsequent years the second percentage would also approach values similar to those of load shedding. Note that the test scenario's balance sheet point of view does not account for any load shedding or curtailment, underlining the necessity of technical simulation for a functioning energy system.

Table 2: Overview of simulation results

Configuration	Load shedding [GWh]	Curtailment [GWh]
Storage + dynamic	64,160.9	9,818.2
Storage + steady-state	71,397.5	20,926.5
No storage + dynamic	88,781.5	84,497.1

The results of the long-term scenario simulation show that a single, well-connected storage site is able to significantly reduce curtailment and improve reliability. It is however not sufficient for a fully feasible and resilient operation of the German hydrogen infrastructure in its currently planned form. The distribution of sinks and sources in relation to the storage and the connecting network between them seems to have a limiting effect on the storage's balancing capability. Solutions to this problem include increasing the number of storage locations, favouring shorter distances to large demands, placing compressors throughout the network to adjust for pressure losses, increasing the grid pressure and a smart, predictive dispatch. It should be noted however, that realistically not all of the load shedding can be mitigated by cavern storage. Especially highly flexible power plants might require smaller, nearby storage solutions in order to satisfy sudden high-power demand spikes. Since large-scale hydrogen storage is limited to a few geologically feasible locations, the interaction with the grid has to be thoroughly understood in order to quantify its capabilities and ensure a resilient infrastructure. The subsequent section aims to investigate this interaction in a systematic manner.

4. Cavern-grid interaction

As shown in section 3, the grid has a limiting effect on the cavern's balancing capability and influences its operation. In order to quantify this interaction and gain a deeper understanding, this section investigates it under synthetic conditions. Since demand spikes and the subsequent load shedding pose a more serious threat to nominal operation than supply volatility, the focus is on the interaction between caverns and loads.

In control theory, a step response analysis is often used to retrieve the dynamic properties of a system. By phrasing an analogy to this for the cavern-grid interaction, information on the flexibility and capability of the storage inside the core network can be obtained. The setup once again involves Etzel as the only storage site and assumes a single sink at one node in the grid. Initially, all flows are set to 0 and the pressure is uniform and at the lower limit of 50 bar. At $t = 0$, the step input, in this case a maximum storage discharge, is triggered. At the same time, the sink withdraws as much hydrogen from the grid as possible. Figure 9 shows the step input by the storage in blue and the resulting response of the sink in red. The storage output is capped at 40 GW, which corresponds to the maximum discharge power of around 100 caverns and is chosen as an upper bound for hydrogen flow from a single site. However, in the example this flow rate can only be maintained for about two hours. During this time, the storage injects more than the network is able to distribute and thus increases the local pressure. Once the upper limit of 70 bar is reached, the storage output has to be throttled. Simultaneously, the sink withdraws any available hydrogen from the grid by keeping its local pressure at the lower limit of 50 bar. As a consequence, the withdrawal power slowly rises and eventually settles in at a final maximum power P_∞, when the system is in equilibrium. Analogous to control theory, the time constant τ of this step response can be determined by finding the time it takes until the sink power reaches 63.2 % of its final value.

Performing the step response analysis for every node in the network yields a heat map of the deliverable power from Etzel into the core grid. As visualised by Figure 10, only the nodes directly adjacent to the storage are able to receive close to the full power. The

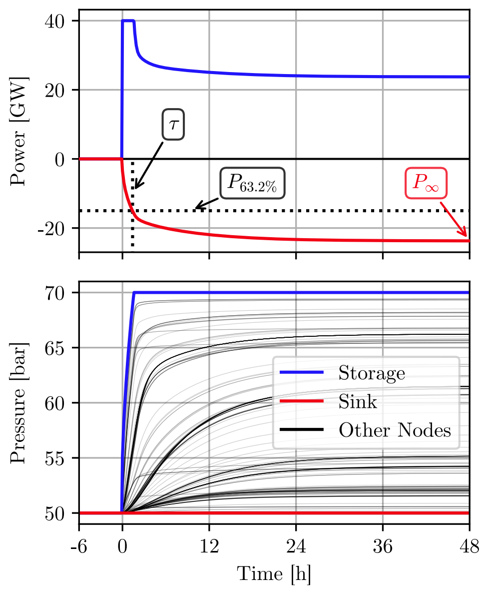

Figure 9: Example of hydrogen flow and grid pressure profiles of the storage node and the sink node during a synthetic two-day maximum load step response benchmark. The remaining grid nodes are shown in black

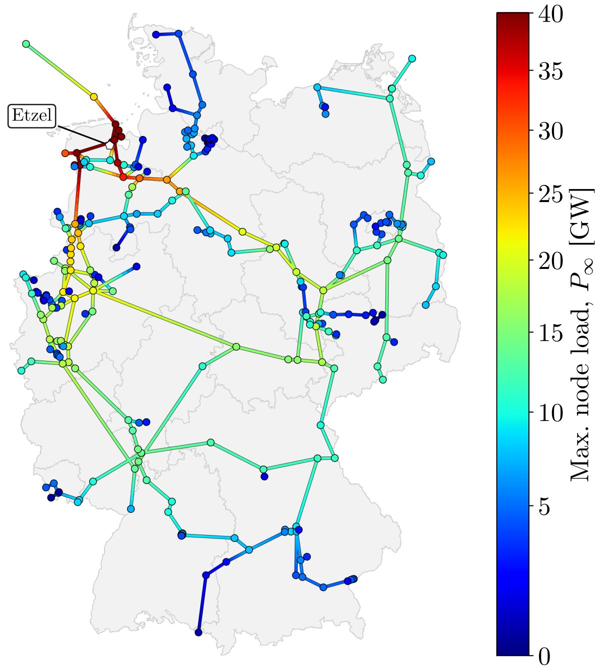

Figure 10: Map of the maximum power the storage site in Etzel can deliver to each node of the German hydrogen core network with a 50-70 bar pressure spread

further away a load is located, the lower the maximum power becomes. This is a direct result of the pressure delta (70-50 bar) having to stretch over larger distances and therefore allowing smaller volume flows. Another factor affecting the flow distribution is pipeline diameter. Bigger pipelines feature a smaller relative pressure drop. Hence, high deliverable power stretches further into the network along these main segments. Conversely, small branch lines, even if located close to the storage, are limited by their reduced diameter and capacity.

It is important to note, that the shown maximum node loads cannot be served in parallel but only in an isolated setup. Analysing the obtained power values, reveals that the storage in Etzel is able to supply individual loads of 10 GW or more in most regions of the network. However, considering the fact that the scenario contains peaks of up to 170 GW (Fig. 4) of distributed demand, it becomes apparent that the grid simply cannot keep up and transport the necessary hydrogen from storage to the sinks under these circumstances.

As flexibility is highly important, especially for the energy sector, the time delay between the storage's reaction to imbalances and availability of additional power in the grid is crucial as well. This delay is quantified by the time constant τ and plotted on the core network in Figure 11. While nearby nodes receive a noticeable power increase within the first hour, far-away sections of the grid have to wait up to eight hours for significant change.

In case the network is not at the lower pressure limit, line pack is able to buffer some of the time until the storage reaction has an effect. The duration however heavily depends on the load and current grid pressure. Big loads will quickly deplete the line pack flexibility and it cannot fully bridge the gap until the additional storage flow reaches the load. To combat this, smart storage dispatch strategies could anticipate flexibility needs and response ahead of time, thus reducing or eliminating the time delay.

Taking the nodes and arranging them in a plot with distance from Etzel on the x-axis and the maximum node load on the y-axis yields Figure 12. This visualisation enables several observations. Firstly, disregarding the colour of the markers, the relation between larger distance to the storage and lower maximum load is confirmed. Secondly, the left-to-right colour gradient from blue to red clearly shows the correlation of storage reaction time and distance. Lastly, the time constant also exhibits minor dependency on the maximum node load and therefore pipeline diameter, indicated by the vertical gradient at medium distances.

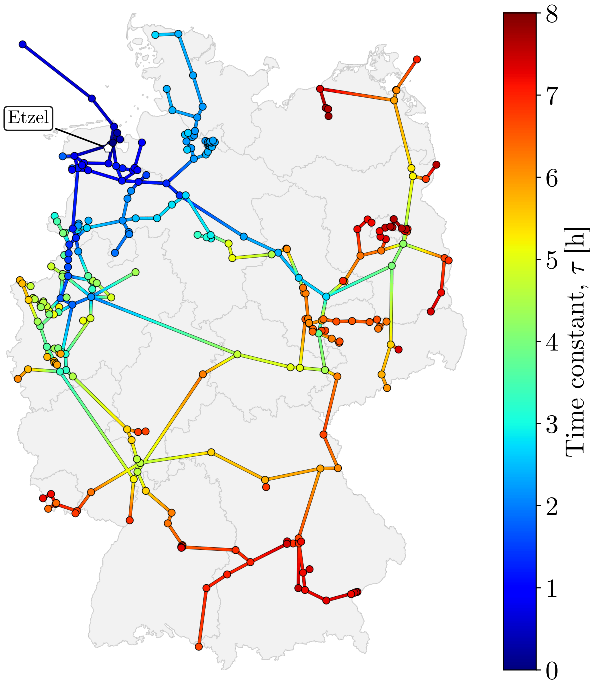

Figure 11: Map of the time delay between a maximum injection from Etzel into the German grid and availability of 63.2 % of the respective maximum load at each node

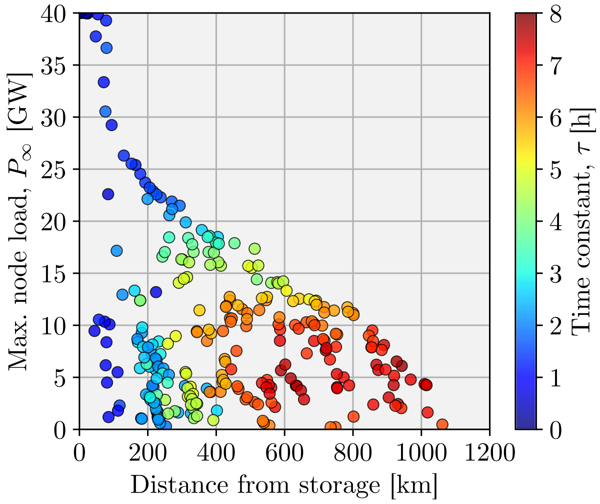

Figure 12: Arrangement of all network nodes by their distance to the storage and maximum deliverable power, showing the correlation between them. The time delay until a significant increase in hydrogen flow reaches each node is shown by the colour scale

While the investigated setup represents a highly synthetic edge case, it serves as a showcase of the limitations the network imposes on cavern storage. It is found that large and volatile loads and supplies require a short distance to the next flexibility provider like a storage. Ideally, the connection uses pipelines with big diameters, which further improves power delivery and reduces delay.

In reality the presence of additional loads and distributed supplies alters the actual pipeline utilization and resulting constraint violations. Depending on the boundary conditions, this could lead to better or worse availability and reaction times. For an exhaustive analysis different critical cases have to be simulated in order to obtain applicable resiliency results.

5. Conclusion

This study introduced DLR-DUST, a Python-based, hydraulic, dynamic gas network simulation tool and coupled it with a numerical cavern model in order to investigate the interaction between these infrastructure components. DLR-DUST was then applied to simulate the German hydrogen system in a 2045 long-term scenario under dynamic conditions. For the analysis, a single storage site was placed in Etzel in north-west Germany. While the balance-sheet point of view in the test scenario provides perfectly balanced hydrogen supply and demand, the simulation results showed that actually around 21 % of the loads and 3 % of the generation have to be curtailed in order to remain within the pressure limits of the grid. Especially the volatile demand of the energy sector is affected by load shedding. Comparison with steady-state results demonstrated the importance of dynamic simulation for accurate design and operation data, as line pack showed a sizeable buffering capability. Further, a comparison with a configuration without any storage quantified the balancing capability of the site in Etzel. It was found to reduce load shedding and supply curtailment by 27 % and 88 %, respectively. Based on this scenario analysis, the interaction between storage in Etzel and the core network was investigated in greater detail. Analogous to control theory, a step response analysis was performed for each node of the network. The outcome provided information about the maximum power delivery from a single storage site into the grid and the time delay until a significant change in hydrogen availability was measured. From this, general correlations were derived. The deliverable power from a storage to any given node is dependent on the distance and the connecting diameters. The latter having the greatest effect, while the distance acts as an upper bound. In contrast, the time constant, i.e. the time it takes until 63.2 % of the maximum power is reached, is only marginally dependent on pipeline diameter but correlates strongly with distance from storage. Since especially the energy sector requires short-term and high-amplitude flexibility, additional nearby storage solutions and/or additional compressor stations would be beneficial.

Overall, the presented results show that a functional and resilient hydrogen infrastructure requires well-connected storage sites and that network and storage have to be considered together. In the example, the single site in Etzel demonstrated substantial potential in balancing supply and demand. However, it was also found that beyond capacity, grid topology and location of loads impact the overall performance. A well-designed system therefore calls for in-depth understanding of the cavern-grid interaction. Especially critical and volatile demands, such as hydrogen-fired power plants, have to be thoroughly analysed in order to guarantee a reliable supply of hydrogen. This involves ensuring sufficient power delivery from storage and acceptable ramping times during all conditions.

Analyses like these can only be conducted with transient models and detailed infrastructure data, thus proving the relevance and importance of dynamic simulation. The major benefit of DLR-DUST compared to other models is the added coupling with a cavern model, which ensures compliance with cavern and surface facility constraints at all times. In combination, this encompasses the core hydrogen infrastructure components and enables resiliency analyses, line pack studies as well as design and operation tuning in great detail.

Building on this study's findings, additional items of research are proposed. A sensitivity analysis of key design and operational parameters on the feasibility of the long-term scenario would provide valuable insight into the improvement potential. Factors like higher pressures or different pressure regions, separated by compressors, could significantly reduce curtailment and load shedding. Furthermore, the implementation of smart dispatch strategies that anticipate demand and supply in the coming hours could more effectively make use of line pack buffering. In a following step, dynamic coupling with the electric infrastructure via electrolysis and hydrogen-fired power plants could be implemented, allowing a full-picture resiliency analysis of the entire energy system. In general, the implementation of a non-linear optimization step, as presented by [22] and [23], would enable examination of different strategies and their impact on resilience as well as infrastructure utilization and overload.

CRediT author statement

Lars Höpken: Conceptualization, Data curation, Methodology, Software, Validation, Visualization, Writing - original draft preparation. **Wiebke Germer**: Conceptualization, Supervision, Project administration, Writing - review and editing. **Hendrik Langnickel**: Conceptualization, Supervision, Project administration, Writing - review and editing. **Alexander Dyck**: Conceptualization, Supervision, Project administration, Funding acquisition, Writing - review and editing. **Carsten Agert**: Conceptualization, Supervision. All authors have read and agreed to the published version of the manuscript.

Acknowledgements

The authors thank Claudia Kröner for her valuable contributions and discussions about boundary conditions and inputs. Furthermore, the authors thank Michael Ebner of the Forschungsstelle für Energiewirtschaft e.V. (FfE) for the friendly provision of scenario data. The authors also thank the Federal Ministry of Economic Affairs and Climate Action for financial support within the project H2CAST-Prove (reference number 03EI3073D) on the basis of a decision by the German Bundestag.

Declaration of interests

The authors declare that they have no known competing financial interests or personal relationships that could have appeared to influence the work reported in this paper.

Declaration of AI and AI-assisted technologies in the writing process

During the preparation of this work, the authors utilized OpenAI's ChatGPT and DeepL's DeepL Write as programming assistants and in order to improve the style of writing. After using these tools/services, the authors reviewed and edited the content as needed and take full responsibility for the content of the publication.

References

[1] Bundesnetzagentur, Genehmigung eines Wasserstoff-Kernnetzes, https://www.bundesnetzagentur.de/DE/Fachthemen/ElektrizitaetundGas/Wasserstoff/_DL/Genehmigung.pdf?__blob=publicationFile&v=6, accessed: 2026-04-20, (2024).

[2] FNB Gas, Hydrogen core network, https://fnb-gas.de/en/hydrogen-transport/hydrogen-core-network/, accessed: 2026-04-20, (2026).

[3] Y. Sagdur, R. Slowinski, R. van Rossum, A. Kozub, L. Kühnen, M. Overgaag, A. Michelet, S. Kandathiparambi, P. London, European hydrogen backbone: Implementation roadmap–cross border projects and costs update, https://ehb.eu/files/downloads/EHB-2023-20-Nov-FINAL-design.pdf, accessed: 2026-04-20, (2023).

[4] Consentec GmbH, Fraunhofer-Institut für System- und Innovationsforschung ISI, ifeu – Institut für Energie- und Umweltforschung Heidelberg, Technische Universität Berlin, Long-term scenarios for the transformation of the energy system in germany, https://langfristszenarien.de/enertile-explorer-wAssets/docs/LFS3_045-Energieangebot_final.pdf, accessed: 2026-04-20, (2024).

[5] D. Stolten, P. Markewitz, T. Schöb, F. Kullmann, S. Risch, T. Groß, M. Hoffmann, D. Franzmann, T. Triesch, S. Kraus, R. Maier, B. Gillessen, H. Heinrichs, N. Pflugradt, T. Grube, J. Linssen, L. Kotzur, Neue Ziele auf alten Wegen? Strategien für eine treibhausgasneutrale Energieversorgung bis zum Jahr 2045, Vol. 577 of Schriften des Forschungszentrums Jülich Reihe Energie & Umwelt / Energy & Environment, Forschungszentrum Jülich GmbH Zentralbibliothek, Verlag, Jülich, 2022.
URL https://juser.fz-juelich.de/record/908382

[6] Agora Think Tanks, Prognos AG, Öko-Institut e.V., Wuppertal Institut für Klima, Umwelt, Energie gGmbH, Universität Kassel, Klimaneutrales Deutschland. Von der Zielsetzung zur Umsetzung – Vertiefung der Szenariopfade, https://www.agora-energiewende.de/fileadmin/Projekte/2023/2023-30_DE_KNDE_Update/A-EW_349_KNDE_Szenariopfade_WEB.pdf, accessed: 2026-04-20, (2024).

[7] D. G. Caglayan, N. Weber, H. U. Heinrichs, J. Linßen, M. Robinius, P. A. Kukla, D. Stolten, Technical potential of salt caverns for hydrogen storage in Europe, International Journal of Hydrogen Energy 45 (11) (2020) 6793–6805. doi:10.1016/j.ijhydene.2019.12.161.

[8] L. Höpken, H. Bekebrok, A. Pluta, H. Langnickel, I. Savchenko, M. Ohm, O. Steinmann, M. Zobel, A. Dyck, C. Agert, Modelling green hydrogen storage in salt caverns: Implications of future storage demands on cavern operation, Journal of Energy Storage 119 (2025) 116150. doi:10.1016/j.est.2025.116150.

[9] Storengy, France Hydrogen Germany, https://frhyge-project.eu/, accessed: 2026-04-22, (2026).

[10] H. Janßen, B. Satola, M. Kroener, A. Dyck, M. Vehse, M. Wark, C. Agert, Assessment of the feasibility of hydrogen storage in salt caverns: Implications for purity and contamination pathways for fuel cell mobility, International Journal of Hydrogen Energy 170 (2025) 151236. doi:https://doi.org/10.1016/j.ijhydene.2025.151236.
URL https://www.sciencedirect.com/science/article/pii/S0360319925042387

[11] STORAG ETZEL GmbH, H2CAST Etzel - Making energy transition work, https://h2cast.com/, accessed: 2026-04-20, (2026).

[12] Initiative Energien Speichern e.V., Stellungnahme zum Antrag für das Wasserstoff-Kernnetz, https://energien-speichern.de/wp-content/uploads/2024/08/INES-Stellungnahme_Antrag_H2-Kernnetz.pdf, accessed: 2026-04-20, (2024).

[13] SIMONE Research Group s.r.o., SIMONE SOFTWARE, https://www.simone.eu/simone-simonesoftware.asp, accessed: 2026-04-27, (2026).

[14] PSI Software SE, PSIganesi/Online, https://www.psi.de/en/solutions/products/psiganesionline, accessed: 2026-04-27, (2026).

[15] encoord Inc., SAInt - An Integrated Systems Modeling Platform, https://www.encoord.com/saint, accessed: 2026-04-27, (2026).

[16] D. Lohmeier, D. Cronbach, S. R. Drauz, M. Braun, T. M. Kneiske, Pandapipes: An open-source piping grid calculation package for multi-energy grid simulations, Sustainability 12 (23) (2020). doi:10.3390/su12239899.
URL https://www.mdpi.com/2071-1050/12/23/9899

[17] Y. Lu, T. Pesch, A. Benigni, Gasnetsim: An open-source package for gas network simulation with complex gas mixture compositions, in: 2022 Open Source Modelling and Simulation of Energy Systems (OSMSES), 2022, pp. 1–6. doi:10.1109/OSMSES54027.2022.9769148.

[18] Q. Chen, A. Guan, F. Chen, W. Huang, A. Jin, M. Gadalla, B. Wang, A transient gas pipeline network simulation model for decoupling the hydraulic-thermal process and the component tracking process, Energy 301 (2024) 131613. doi:10.1016/j.energy.2024.131613.
URL https://www.sciencedirect.com/science/article/pii/S0360544224013860

[19] Y. Lu, A. Ivan Sulimro, T. Pesch, A. Benigni, Fast and scalable dynamic gas network modeling and simulation framework with gas composition tracking, IEEE Access 13 (2025) 104220–104232. doi:10.1109/ACCESS.2025.3579340.

[20] Y. Huang, L. Feng, An equivalent dynamic gas network model with electricity–gas systems, Industrial & Engineering Chemistry Research 62 (30) (2023) 11905–11916. arXiv:https://doi.org/10.1021/acs.iecr.3c01276, doi:10.1021/acs.iecr.3c01276.
URL https://doi.org/10.1021/acs.iecr.3c01276

[21] D. Zhou, X. Jia, S. Ma, T. Shao, D. Huang, J. Hao, T. Li, Dynamic simulation of natural gas pipeline network based on interpretable machine learning model, Energy 253 (2022) 124068. doi:10.1016/j.energy.2022.124068.
URL https://www.sciencedirect.com/science/article/pii/S0360544222009719

[22] R. Burlacu, H. Egger, M. Groß, A. Martin, M. E. Pfetsch, L. Schewe, M. Sirvent, M. Skutella, Maximizing the storage capacity of gas networks: a global minlp approach, Optimization and Engineering 20 (2) (2019) 543–573. doi:10.1007/s11081-018-9414-5.

[23] S. K. K. Hari, K. Sundar, S. Srinivasan, A. Zlotnik, R. Bent, Operation of natural gas pipeline networks with storage under transient flow conditions, IEEE Transactions on Control Systems Technology 30 (2) (2022) 667–679. doi:10.1109/TCST.2021.3071316.

[24] K. A. Pambour, R. Bolado-Lavin, G. P. Dijkema, An integrated transient model for simulating the operation of natural gas transport systems, Journal of Natural Gas Science and Engineering 28 (2016) 672–690. doi:10.1016/j.jngse.2015.11.036.
URL https://www.sciencedirect.com/science/

article/pii/S1875510015302766
[25] K. Pambour, Modelling, simulation and analysis of security of supply scenarios in integrated gas and electricity transmission networks, Ph.D. thesis, University of Groningen (2018). URL https://research.rug.nl/en/publications/modelling-simulation-and-analysis-of-security-of-supply-scenarios
[26] G. Golub, C. Van Loan, Matrix Computations, Johns Hopkins Studies in the Mathematical Sciences, Johns Hopkins University Press, 1996.
[27] I. H. Bell, J. Wronski, S. Quoilin, V. Lemort, Pure and pseudo-pure fluid thermophysical property evaluation and the open-source thermophysical property library coolprop, Industrial & Engineering Chemistry Research 53 (6) (2014) 2498–2508. arXiv:http://pubs.acs.org/doi/pdf/10.1021/ie4033999, doi:10.1021/ie4033999. URL http://pubs.acs.org/doi/abs/10.1021/ie4033999
[28] E. Walter, H. Gehringer, H. Holm, et al., Technische Formeln, 30. Auflage, Fachbuchverlag Leipzig, 1991.
[29] Bundesamt für Kartographie und Geodäsie, Digitales Geländemodell Gitterweite 200 m (DGM200), https://gdz.bkg.bund.de/index.php/default/digitale-geodaten/digitale-gelandemodelle/digitales-gelandemodell-gitterweite-200-m-dgm200.html, accessed: 2026-05-08, (2019).
[30] EMODnet Bathymetry Consortium , EMODnet Digital Bathymetry (DTM 2024), accessed: 2026-05-08, (2024). doi:10.12770/cf51df64-56f9-4a99-b1aa-36b8d7b743a1.
[31] German Federal Government, Climate Change Act, https://www.gesetze-im-internet.de/ksg/KSG.pdf, accessed: 2026-05-11, (2024).
[32] Consentec GmbH, Fraunhofer-Institut für System- und Innovationsforschung ISI, ifeu – Institut für Energie- und Umweltforschung Heidelberg, Technische Universität Berlin, Long-term Scenarios 3 - Scientific analyses on the decarbonization of Germany, https://langfristszenarien.de/enertile-explorer-en/, accessed: 2026-05-08, (2025).
[33] S. Alibas, F. Ausfelder, D. Ditz, M. Ebner, V. Engwerth, T. Fleiter, J. Fragoso García, L. Genge, M. Greitzer, S. Haas, M. Haendel, C. Hank, P. Hauser, M. Heneka, W. Heineken, J. Hildebrand, V. Isik, W. Köppel, R. Harper, M. Jahn, B. Klaassen, T. M. Kneiske, S. Malzkuhn, B. Kuzyaka, T. Mielich, B. Lux, A. Maghnam, F. Müsgens, F. Mendler, A. Pleier, J. Müller-Kirchenbauer, A.-M. Isbert, D. Ruprecht, P. Sadat-Razavi, F. Neuner, B. Pfluger, S. Mohr, M. Ragwitz, M. Scheffler, M. D. Solomon, C. Voglstätter, B. Weißenburger, European hydrogen infrastructure planning (2024). doi:10.24406/publica-2733. URL https://publica.fraunhofer.de/handle/publica/462539
[34] Forschungsstelle für Energiewirtschaft e. V., FfE Open Data Portal, https://opendata.ffe.de/, accessed: 2026-05-11, (2025).
[35] FfE München, Load Curves of the Industry Sector including Feedstock (Europe NUTS-3), https://opendata.ffe.de/dataset/load-curves-of-the-industry-sector-including-feedstock-europe-nuts-3, accessed: 2026-05-08, (2025).
[36] FfE München, Hydrogen production by electrolysis after InfraInt optimization in Europe based on the TransHyDE-Sys stakeholder scenario (2025).
[37] Consentec GmbH, Fraunhofer-Institut für System- und Innovationsforschung ISI, ifeu – Institut für Energie- und Umweltforschung Heidelberg, Technische Universität Berlin, O45 scenarios: Dashboard Hydrogen Dispatch, https://enertile-explorer.isi.fraunhofer.de:8443/open-view/65723/47ff42aaf4d26755dc5a7a0bf91500cf, accessed: 2025-12-15, (2025).